

Central Lancashire Online Knowledge (CLoK)

Title	Early propagation of energetic particles across the mean field in turbulent plasmas
Type	Article
URL	https://clock.uclan.ac.uk/18527/
DOI	##doi##
Date	2017
Citation	Laitinen, Timo Lauri mikael orcid iconORCID: 0000-0002-7719-7783, Dalla, Silvia orcid iconORCID: 0000-0002-7837-5780 and Marriott, D. (2017) Early propagation of energetic particles across the mean field in turbulent plasmas. Monthly Notices of the Royal Astronomical Society, 470 (3). pp. 3149-3158. ISSN 0035-8711
Creators	Laitinen, Timo Lauri mikael, Dalla, Silvia and Marriott, D.

It is advisable to refer to the publisher's version if you intend to cite from the work. ##doi##

For information about Research at UCLan please go to <http://www.uclan.ac.uk/research/>

All outputs in CLoK are protected by Intellectual Property Rights law, including Copyright law. Copyright, IPR and Moral Rights for the works on this site are retained by the individual authors and/or other copyright owners. Terms and conditions for use of this material are defined in the <http://clock.uclan.ac.uk/policies/>

Early propagation of energetic particles across the mean field in turbulent plasmas

T. Laitinen,^{*} S. Dalla^{*} and D. Marriott

Jeremiah Horrocks Institute, University of Central Lancashire, Preston PR1 2HE, UK

Accepted 2017 June 14. Received 2017 June 14; in original form 2017 April 10

ABSTRACT

Propagation of energetic particles across the mean field direction in turbulent magnetic fields is often described as spatial diffusion. Recently, it has been suggested that initially the particles propagate systematically along meandering field lines, and only later reach the time-asymptotic diffusive cross-field propagation. In this paper, we analyse cross-field propagation of 1–100 MeV protons in composite 2D-slab turbulence superposed on a constant background magnetic field, using full-orbit particle simulations, to study the non-diffusive phase of particle propagation with a wide range of turbulence parameters. We show that the early-time non-diffusive propagation of the particles is consistent with particle propagation along turbulently meandering field lines. This results in a wide cross-field extent of the particles already at the initial arrival of particles to a given distance along the mean field direction, unlike when using spatial diffusion particle transport models. The cross-field extent of the particle distribution remains constant for up to tens of hours in turbulence environment consistent with the inner heliosphere during solar energetic particle events. Subsequently, the particles escape from their initial meandering field lines, and the particle propagation across the mean field reaches time-asymptotic diffusion. Our analysis shows that in order to understand solar energetic particle event origins, particle transport modelling must include non-diffusive particle propagation along meandering field lines.

Key words: diffusion – magnetic fields – turbulence – Sun: particle emission.

1 INTRODUCTION

Understanding the propagation of energetic particles in turbulent plasmas is the key for understanding the acceleration of solar energetic particles (SEPs), and their relation to the complex phenomena during solar eruptions. The propagation of these charged particles is affected by the heliospheric electric and magnetic fields. The particles are guided by the Parker spiral field, and experience guiding centre drifts across the field (e.g. Marsh et al. 2013). The turbulent fluctuations in the magnetic field, on the other hand, bring a stochastic element to the propagation of the particles, often modelled as diffusion along and across the mean field direction (Parker 1965).

Energetic particle propagation across the mean magnetic field in turbulent plasmas has been considered as mainly the effect of particles following the meandering field lines (e.g. Jokipii 1966). Current approaches aiming to quantify this effect take into account scattering of the particles along the field lines (Matthaeus et al. 2003; Shalchi 2010). Also the decoupling of the particles from the field lines has been considered (Fraschetti & Jokipii 2011; Ruffolo et al. 2012). These theoretical approaches work towards a time-asymptotic description of particle cross-field transport as a spa-

tial diffusion process. Cross-field diffusion description has recently been applied also in modelling the SEP propagation in the heliosphere (Zhang, Qin & Rassoul 2009; Dröge et al. 2010; He, Qin & Zhang 2011; Tautz, Shalchi & Dosch 2011; Giacalone & Jokipii 2012; Qin et al. 2013; Strauss, Dresing & Engelbrecht 2017).

However, Laitinen, Dalla & Marsh (2013) noted recently that early in the propagation history, particles propagate systematically along meandering field lines, spreading efficiently across the mean field direction (see also Tooprakai et al. 2016). This spreading is non-diffusive in nature, and only at later times the particles decouple sufficiently from their meandering field lines, resulting in propagation that can be described as diffusion across the mean magnetic field. Using full-orbit particle simulations in a Cartesian geometry, Laitinen et al. (2013) concluded that the temporal and spatial evolution of impulsively injected 10 MeV protons, as recorded 1 au from the injection region, remained inconsistent with diffusion description for ~ 20 h after the particle injection. Thus, the non-diffusive early propagation may be very significant to the propagation of the SEPs from the Sun to the Earth. Laitinen et al. (2016) showed that the wide SEP events observed with multiple spacecraft at different heliographic longitudes at 1 au (e.g. Dresing et al. 2012; Lario et al. 2013; Wiedenbeck et al. 2013; Cohen et al. 2014; Dresing et al. 2014; Richardson et al. 2014) could be explained using this approach with particle transport parameters consistent with the

^{*} E-mail: tmlaitinen@uclan.ac.uk (TL); sdalla@uclan.ac.uk (SD)

interplanetary turbulence properties already with a narrow source at the Sun.

The initial study by Laitinen et al. (2013) addressed only one set of particle and turbulence parameters, and did not explore the parameter space of particle and turbulence further to identify properties that may influence the initial non-diffusive particle propagation phase. In this work, we will study the initial non-diffusive phase and the asymptotic diffusive phase in more detail, varying both the particle and turbulence parameters. We will study the nature of the transition from the initial to the asymptotic phase guided by the findings of Laitinen & Dalla (2017), who used a novel method to quantify how the particles are displaced from the meandering field lines and discovered that initially the particles are tied to their meandering field lines well, and decouple only at later stages. We explain the particle simulations and the analysis methods in Section 2 and Appendix A, present our results and discuss their relevance in Sections 3 and 4, and draw our conclusions in Section 5.

2 MODEL

The particles are simulated in magnetic field given by

$$\mathbf{B}(x, y, z) = B\hat{z} + \delta\mathbf{B}(x, y, z), \quad (1)$$

where B is a constant background field, along the z -axis, for which we use the value 5 nT, consistent with magnetic field at 1 au. The fluctuating component $\delta\mathbf{B}(x, y, z)$ consists of Fourier modes, and is constructed using the method presented in Giacalone & Jokipii (1999), and fulfills $\nabla \cdot \mathbf{B} = 0$. We use a composite model, where turbulence is composed of slab and 2D components, at a power ratio 20 per cent:80 per cent. The turbulence is axisymmetric, with axisymmetric distribution of polarization and wave vector directions. The turbulence amplitude is parametrized by using the relative amplitude $\delta B^2/B^2$, where δB^2 is the variance of the fluctuations. The turbulence spectrum for the 2D component follows the Kolmogorov scaling, whereas for the slab component we use spectral indices $q_{\parallel} = 5/3$ and 1.

The full-orbit particle simulations follow the same approach as Laitinen, Dalla & Kelly (2012). We start the particles in a large volume, to reduce the effect of local magnetic field structures, but within the analysis the particle location at time t is determined relative to each particle's initial position. The particles are injected into the simulation as a beam, with pitch angle cosine $\mu = 1$, and simulated for 60 h.

The slab spectral index affects the particles' parallel scattering mean free path, which from quasi-linear theory (Jokipii 1966) varies as $\lambda_{\parallel} \propto R^{2-q_{\parallel}}$, where R is the particle rigidity. In addition, the turbulence energy for the spectra with the two slab spectral indices, $q_{\parallel} = 5/3$ and 1, results in a different scattering power at the resonant scales of the particles simulated in this study. We show λ_{\parallel} as determined from the particle simulations in Fig. 1, for the two spectral indices and $\delta B^2/B^2 = 0.1$. The trends of λ_{\parallel} as function of proton energy for the two slab spectral indices, depicted with the fitted power-law curves, with $E^{0.11}$ and $E^{0.44}$ for $q_{\parallel} = 5/3$ and 1, respectively, are consistent with the quasi-linear theory result. The mean free paths presented in Fig. 1 are consistent with those obtained using interplanetary turbulence properties (e.g. Pei et al. 2010; Laitinen et al. 2016; Strauss et al. 2017) and SEP observation analysis (e.g. Palmer 1982; Torsti, Riihonen & Kocharov 2004).

We analyse the cross-field extent of the particle distribution as a function of the distance along the mean field direction, using

$$\sigma_{\perp}^2(z, t) = \langle (x(z, t) - \langle x(z, t) \rangle)^2 \rangle, \quad (2)$$

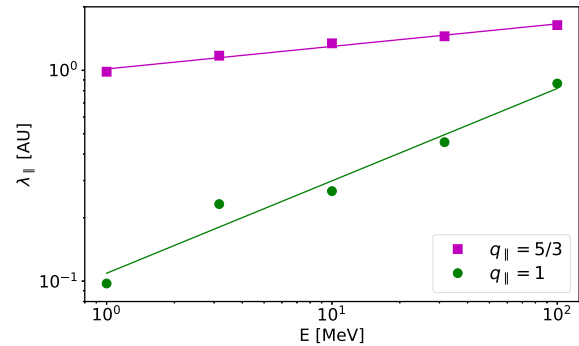


Figure 1. The parallel mean free path of protons at energies 1–100 MeV for turbulence with $\delta B^2/B^2 = 0.1$. The curves show the power-law fits to the mean free paths, with trends $E^{0.11}$ and $E^{0.44}$ for $q_{\parallel} = 5/3$ and 1, respectively.

where $\langle \rangle$ represents the ensemble average of particles. The use of x instead of y is arbitrary, and due to the axisymmetry of the turbulence has no effect on the obtained values. Also deviations in $r_{\perp} = \sqrt{x^2 + y^2}$ could be considered, however, it would complicate comparing our results with other work, which typically consider Cartesian deviations and diffusion coefficients. We also note that equation (2) calculates the deviations with respect to the mean, $\langle x(z, t) \rangle$, in order to eliminate the effects due to the potential asymmetries of the distributions (see Figs 2 and 3) that arise from finite range of fluctuation scales used in the simulations.

The form of the equation (2) differs from the conventional definitions in that $\sigma_{\perp}^2(z, t)$ is defined for particles at a given field-parallel distance z at time t , instead of for all particles in the simulation. This choice is motivated by observations: we do not observe the full 3D distribution of the particles, but rather sample the particle distribution in fixed points in space. Recent observations of SEPs by the *STEREO*, *SOHO* and *ACE* spacecraft have provided us with a view of the longitudinal extent of SEP events at 1 au from the Sun. Our definition of σ_{\perp}^2 aims to provide comparison of simulated particle transport with these measurements.

3 RESULTS

In this section, we will first view the qualitative behaviour of the particle population along and across the mean field direction for different particle and turbulence parameters. We will then proceed to quantify the evolution of the particle population's extent, using simple considerations presented in Appendix A.

As a first step in forming a view on the evolution of particle population along and across the mean field, we present a contour plot of the proton density in Fig. 2, for turbulence with $\delta B^2/B^2 = 0.1$ and $q_{\parallel} = 5/3$ for four different proton energies. The distributions are integrated in y -direction to reduce numerical noise in the contours. The distributions are shown at times when a non-scattered proton of the given energy would have propagated the distance of $z_{\text{ns}} = 2$ au, $t = z_{\text{ns}}/v$. Thus, the four panels depict the distribution of particles of different energies that would have travelled the same distance, unscattered, in a constant background magnetic field. The sharp decrease and narrowing of the particle distribution near $z_{\text{ns}} = 2$ au demonstrates the finite propagation distance of the particles and the longer distance travelled by particles along meandering field lines to larger cross-field distances in the x -direction. The decrease starts already before $z = 2$ au, as some of the first particles have experienced scattering due to the small-scale turbulence.

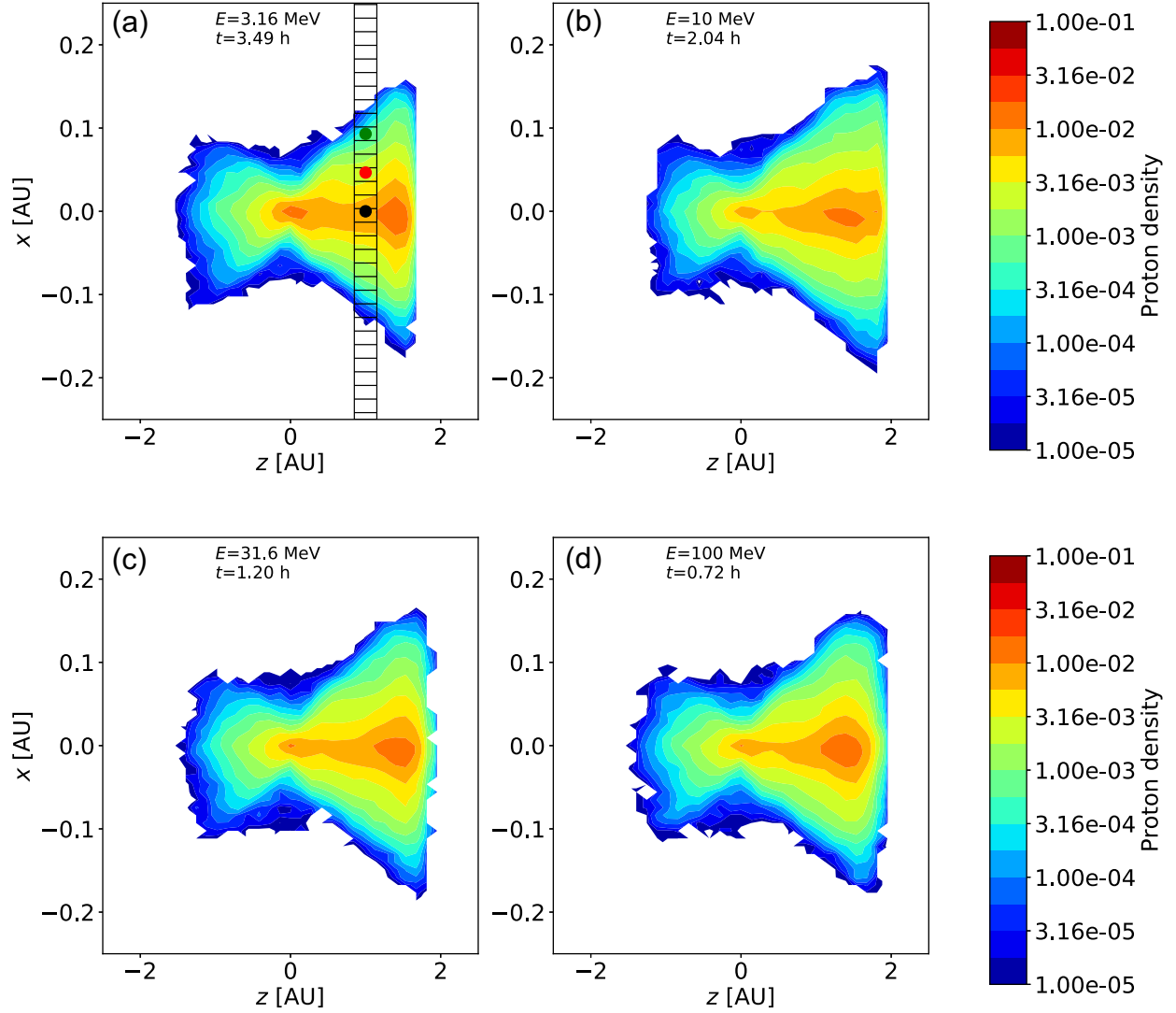


Figure 2. Contours of the spatial distributions of protons with energies of 3.16, 10, 31.6 and 100 MeV, with turbulence parameters $\delta B^2/B^2 = 0.1$ and $q_{\parallel} = 5/3$. The contours are given at the times when an unscattered proton of the given energy would have propagated a distance of 2 au. The circles in panel (a) depict positions corresponding to curves in Fig. 4, and the hatched box at 1 au the region used for determining $\sigma_{\perp}^2(z = 1 \text{ au}, t)$.

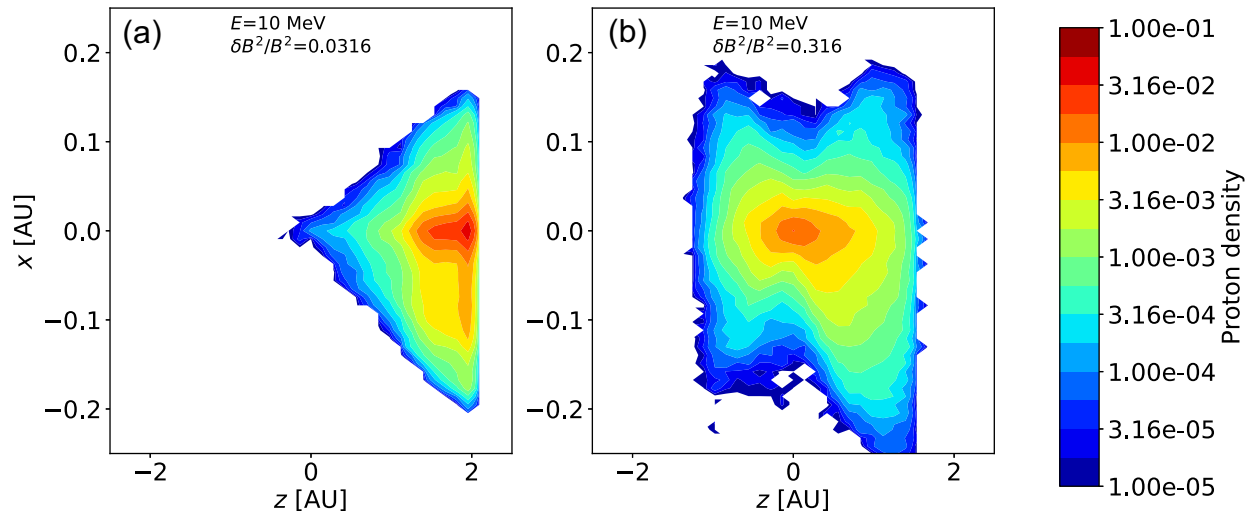


Figure 3. Contours of the spatial distributions of 10 MeV protons with turbulence amplitudes 0.003 16 and 0.316, and $q_{\parallel} = 5/3$. The contours are given at the times when the times when an unscattered proton of the given energy would have propagated a distance of 2 au, at $t = 2.04$ h.

As can be seen in Fig. 2, the particles spread rapidly from their point of origin in the cross-field direction (vertical axis): the front of the fastest propagation particles at $z = 2$ au is much wider than at $z = 0$ au. A small number of backscattered particles have advanced to the region $z < 0$ au (on horizontal axis), and show also expansion in the cross-field direction faster than that at $z = 0$ au. As discussed in Laitinen et al. (2013), the resulting butterfly-shape of particle distribution cannot be obtained by a simple diffusive spreading of particles. In addition, the distribution of the particles at different distances along the field direction is qualitatively very similar at all energies. This suggests that the particles with different energies are propagating along the same pathways.

In Fig. 3, we show the distribution of 10 MeV protons in turbulence of different strength, $\delta B^2/B^2 = 0.0316$ and $\delta B^2/B^2 = 0.316$ in panels (a) and (b), respectively. The distributions are again shown at the time when an unscattered particle would have reached 2 au along a uniform magnetic field. The distributions differ significantly at $z < 0$ au where the number of backscattered particles decreases as the turbulence weakens, with almost no backscattered particles for the weakest turbulence case, $\delta B^2/B^2 = 0.0316$ (Fig. 3a). On the other hand, at $z \sim 2$ au the particles propagating in weaker turbulence (3a) have progressed further in parallel direction, remaining in a more coherent pulse. These differences are due to the dependence of parallel scattering rate on the turbulence amplitude. For 10 MeV protons, the quasi-linear parallel mean free path, obtained from the simulated particles, is $\lambda_{\parallel} = 0.29$ au for the case of $\delta B^2/B^2 = 0.316$ (Fig. 3b), consistent with considerable scattering along the mean magnetic field by the time the particles have propagated for a time corresponding to scatter-free propagation of 2 au. For the case of $\delta B^2/B^2 = 0.0316$, the mean free path is $\lambda_{\parallel} = 7.6$ au, resulting in the almost scatter-free propagation depicted in Fig. 3(a). For the intermediate case, $\delta B^2/B^2 = 0.1$, depicted in Fig. 2(b), the mean free path is $\lambda_{\parallel} = 1.3$ au, which can be seen in some parallel diffusion and backscattering of the particles.

The cross-field extent of the particle distribution also appears to depend on the turbulence amplitude, as seen when comparing Figs 3(a), 2(b) and 3(b), for the weak, intermediate and strong scattering conditions, respectively, for 10 MeV protons. The distribution is clearly narrower at lower turbulence amplitude turbulence at $z = 0$ au. A similar trend is seen also at larger distances along the mean field line direction: at $z = 2$ au, the weak turbulence case, as presented in Fig. 3(a), the particles are much more concentrated on a narrow cross-field extent than in the more turbulent cases presented in Figs 2(b) and 3(b).

In Fig. 4, we show the time development of the particle density, as it would be measured by spacecraft situated at the black, red and green circles in Fig. 2(a), for 1 and 100 MeV protons (solid and dashed curves), respectively. As can be seen, the particle density decreases strongly when the measuring point is moved from the black circle, connected along the mean magnetic field to the particle source, across the mean field direction, to the red and green circles. However, the ratio of intensities at different locations appears to be initially independent of time (at times < 1 h for 100 MeV protons, and < 10 h for 1 MeV protons), and only at later times the intensities at different locations begin to converge. This behaviour of initially time-independent cross-field distribution is seen at both energies in Fig. 4. Furthermore, the temporal behaviour in the initial phase of the simulations, when scaled with the particle velocity, is very similar. Thus, the initial cross-field spreading of the particles seems to be independent of both energy and velocity-scaled time. At later times, the intensities at different locations begin to converge, as the width of the particle population increases.

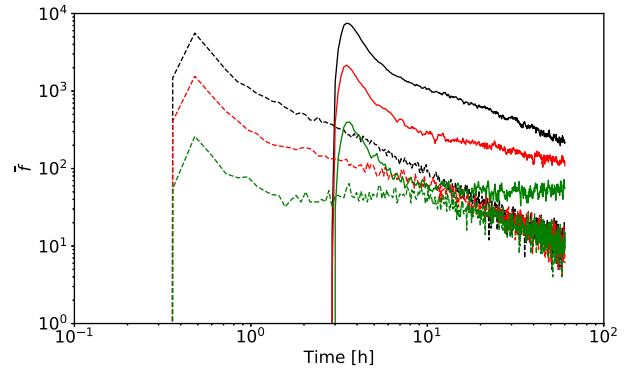


Figure 4. The time evolution of the distribution of protons at $z = 1$ au and $x = 0, 0.046$ and 0.093 au from (black, red and green curves, respectively), for 1 and 100 MeV (solid and dashed curves, respectively), and $\delta B^2/B^2 = 0.1$ and $q_{\parallel} = 5/3$.

To analyse the particle cross-field extent quantitatively, we study the temporal evolution of the cross-field variance of the particles, $\sigma_{\perp}^2(z, t)$, as a function of time at different distances from the particle source. As discussed in the previous section, we define the cross-field variance for particles at a given distance along the mean field direction using equation (3), so that, for example, the variance $\sigma_{\perp}^2(z = 1 \text{ au}, t = 3.49 \text{ h})$ is determined from the particles within the hatched box in Fig. 2(a).

In Fig. 5, we show $\sigma_{\perp}^2(z, t)$ at $z = 0.56$ au (top panel) and $z = 2.09$ au (bottom panel), as a function of time, for 1, 3.16, 10, 31.6 and 100 MeV protons, from the right- to left-hand side, respectively. The black curves represent a fitted function that is discussed below. As we can see, the temporal behaviour of the cross-field variance of the particles can be decomposed into three time periods. The first time period, visible only for 1 MeV protons in Fig. 5 (blue, rightmost curve) demonstrates fast increase of the variance to a constant level (at times < 2 h in the top panel). This is caused by the fact that the particles with very small cross-field deviation are likely to have the shortest path-lengths along the meandering field lines, and thus the first particles will arrive earlier to the well-connected location ($x = 0$ au in Figs 2 and 3) than to larger cross-field deviations. The effect of the length of the meandering fieldlines on the particle onsets at different spatial locations will be investigated in a separate study.

The first time period is short, and due to finite time sampling of the particle locations within the simulations, it is not visible at higher energies. After the initial fast rise, the variance remains at a constant level for a considerably long time, at about $\sigma_{\perp}^2(z, t) = 38 r_{\odot}^2$ at $z = 0.56$ au and $130 r_{\odot}^2$ at $z = 2.09$ au. The constant level is independent of energy, and increases with distance along the mean magnetic field direction (top versus bottom panel of Fig. 5).

Subsequently, the cross-field extent of the particle population begins to increase and finally reaches a time-asymptotic $\sigma_{\perp}^2 \propto t$ trend, consistent with diffusive cross-field spreading of the particles. Both the onset time and the time profile of the change from constant to the diffusive phase depend on both the particle energy and the distance along the z -axis. The simplest method of obtaining the time when the cross-field diffusion becomes significant, t_a , is to use time at which the time-asymptotic straight line $\sigma_{\perp}^2 \propto t$ intersects the initial constant value of σ_{\perp}^2 level (the magenta and black dashed lines in Fig. A1, respectively).

The simplest approach to describe mathematically, the temporal behaviour of the cross-field variance presented in Fig. 5 would be

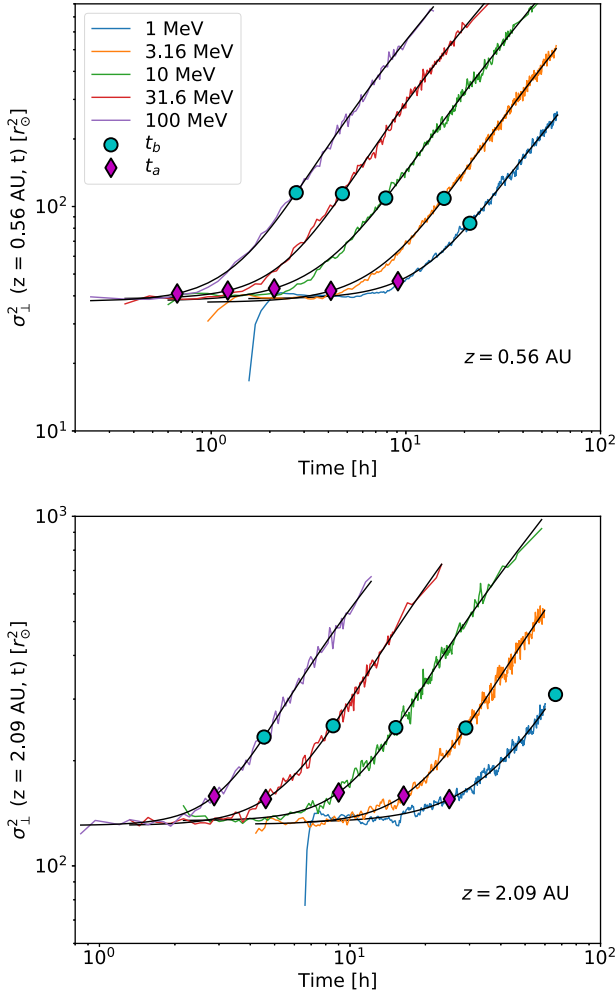


Figure 5. The mean square width of protons at 0.56 au (top panel) and 2.09 au along the mean field direction from the source location. The black curves show fits made using equation (3), the magenta diamond the time t_a and the cyan circle the time t_b . The turbulence parameters are $\delta B^2/B^2 = 0.1$ and $q_{\parallel} = 5/3$.

to consider a diffusive spreading of particles from the meandering field lines with constant diffusion coefficient, which would result in variance given by equation (A5). While such a model is easy to implement and can be used as the first approach, as in, for example, Laitinen et al. (2016), we will consider here an improvement to the modelling of the transition, based on the work by Laitinen & Dalla (2017). In Appendix A, we derive a model with time-dependent diffusion coefficient, which will justify fitting the variance with functional forms such as equation (A6). In this work, we will use

$$\sigma_{\perp}^2(z, t) = \sigma_{\perp 0}^2(z) + \frac{\sigma_{\perp 1}^2(z) t / t_0}{1 + [t_b(z) / t]^{\alpha(z) - 1}}, \quad (3)$$

where $\sigma_{\perp 0}^2(z)$ is the early-time constant cross-field variance of the particles at distance z , $t_0 = 1$ h the unit of time, $t_b(z)$ is the onset time of the time-asymptotic diffusive regime and $\alpha(z)$ the power-law index that describes the fast spreading of the particle population before t_b . The time-asymptotic diffusive rate of change of the cross-field variance of the particle population is given by $\sigma_{\perp 1}^2(z) / t_0 \equiv 2 \kappa_{\perp}(t \gg t_b)$, with $\kappa_{\perp}(t)$ the time-dependent particle diffusion coefficient (see Appendix A). Using the parameters in

equation (3), $t_a = \sigma_{\perp 0}^2 / \sigma_{\perp 1}^2 t_0$. The times t_a and t_b , and their relation to the $\sigma_{\perp}^2(z, t)$ curve and its asymptotes are shown in Fig. A1, and are further discussed in Appendix A.

It should be noted that equation (3) is of the same form as the fitting function used in Laitinen & Dalla (2017), at the limit of $t \gg t_1$ in their formulation. Here, we exclude the early behaviour, $t \lesssim t_1$ discussed in Laitinen & Dalla (2017), as displacements of order Larmor radius are too small to be seen in our current analysis.

We fit equation (3) to the cross-field variances from our simulations at different distances $z = 0.3$ –3 au, and study the dependence of the fit parameters on z , the particle energy and the turbulence properties. We exclude fits where the relative error of any of the fit parameters in equation (3) exceeds 10 per cent. As an example, we show the fits of the simulation results with equation (3) in Fig. 5 with black curves, with t_b shown with a cyan circle. As can be seen, equation (3) mostly fits the simulation results well at all energies on both locations.

In Fig. 6, we show the evolution of the fit parameters as a function of z for five proton energies for turbulence parameters $\delta B^2/B^2 = 0.1$ and $q_{\parallel} = 5/3$. Panel (a) shows the early-time constant cross-field variance $\sigma_{\perp 0}^2$, which increases approximately linearly as a function of distance. The $\sigma_{\perp 0}^2(z)$ curves for different energies overlay each other almost perfectly, suggesting that the spread of particles is caused by the diffusive spreading of the meandering magnetic field lines, rather than particle scattering in space across the mean field.

In Fig. 6(b), we show $\sigma_{\perp 1}^2$, which describes the time-asymptotic diffusive spreading rate of the particles. As can be seen, $\sigma_{\perp 1}^2$ is clearly energy-dependent, and almost independent of z , as expected for diffusive spreading of particles. We determined that $\sigma_{\perp 1}^2$ is roughly proportional to the particle velocity, and is also consistent with the dependence $\kappa_{\perp} \propto R^{10/9}$ of the particle diffusion coefficient on rigidity given by the Nonlinear Guiding Center (NLGC) theory (Matthaeus et al. 2003; Shalchi, Bieber & Matthaeus 2004).

In Fig. 6(c), we show t_b , which represents the onset time of the diffusive spreading of particles. A closer inspection shows that the onset time is roughly proportional to the inverse of velocity. Similar scaling was found by Laitinen & Dalla (2017), who noted that the transition time-scale from the slow to fast diffusive spreading at $z = 0$ au is proportional to the parallel scattering time-scale $\tau_{\parallel} \propto v^{-2/3}$.

However, as can be seen in Fig. 6, the onset time t_b is not independent of the distance z , but increases slowly, inconsistent with the assumptions of the simple diffusion model described in equation (A6). The inconsistency can be caused by the finite propagation time of the particles to distance z , not taken into account in equation (A6).

In Fig. 6(c), we also show the asymptotic time t_a , with the thin dashed curves. As can be seen, t_a approaches and surpasses t_b at larger distances. As discussed in Appendix A, the determination of t_b and α are unreliable when t_a approaches t_b , and the unreliable values of t_b are not shown in Fig. 6(c).

Fig. 6(d) shows the parameter α , which describes the fast spreading of the particles until the time-asymptotic diffusive phase is reached. As interpreted by Laitinen & Dalla (2017), the fast spreading begins when the particles cease being well tied to their field lines. The onset time of the fast spreading phase, denoted by t_1 in Laitinen & Dalla (2017), however, is masked by the early-time $\sigma_{\perp 0}^2$ (see Fig. 5), and can only be quantified using the method described in Laitinen & Dalla (2017). The α in Fig. 6(d) shows no clear energy dependence, consistent with Laitinen & Dalla (2017).

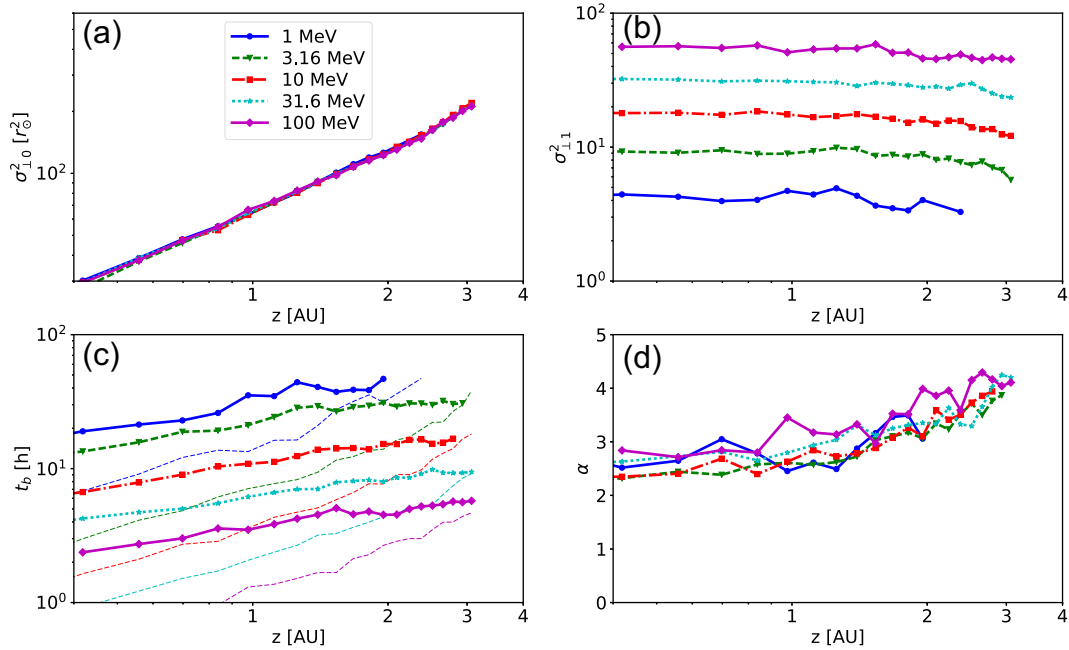


Figure 6. The fitting parameters of the equation (3) to the cross-field particle distribution variances at different distances, for protons of energies 1–100 MeV propagating in turbulence with $\delta B^2/B^2 = 0.1$ and $q_{\parallel} = 5/3$. (a) the early-time cross-field variance of the distribution, $\sigma_{\perp 0}^2$; (b) the asymptotic long-time behaviour $\sigma_{\perp 1}^2$; (c) the turnover time t_b (thick curves) and the asymptotic behaviour changing time t_a (thin dashed curves); and (d) the power-law index α .

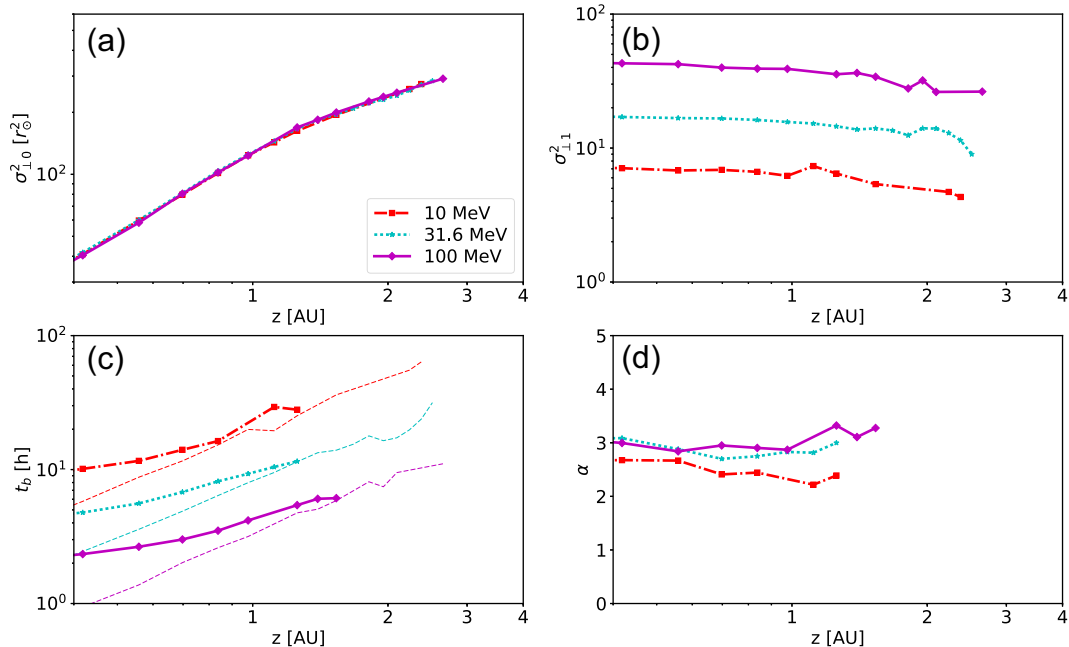


Figure 7. The fitting parameters of the equation (3) to the cross-field particle distribution variances at different distances, for proton energies 10–100 MeV propagating in turbulence with $\delta B^2/B^2 = 0.1$ and $q_{\parallel} = 1$. (a) the early-time cross-field variance of the distribution, $\sigma_{\perp 0}^2$; (b) the asymptotic long-time behaviour $\sigma_{\perp 1}^2$; (c) the turnover time t_b (thick curves) and the asymptotic behaviour changing time t_a (thin dashed curves); and (d) the power-law index α .

In Fig. 7, we show the simulation fit parameters for particles in turbulence with slab spectral index $q_{\parallel} = 1$. The fit of the variance with equation (3) could be successfully performed only for energies in the range of $E = 10$ –100 MeV. For lower energy protons, the cross-field variance remained almost constant for the simulation period of 60 h.

In panel (a) we can see that the early-time, constant cross-field variance $\sigma_{\perp 0}$ is independent of energy also for $q_{\parallel} = 1$. This energy-independence was evident also for energies <10 MeV, for which the fitting of equation (3) was not successful. In panel (b), we note that $\sigma_{\perp 1}^2$ is again almost independent of z . However, its dependence on energy is different than in the case $q_{\parallel} = 5/3$ (Fig. 6b): The

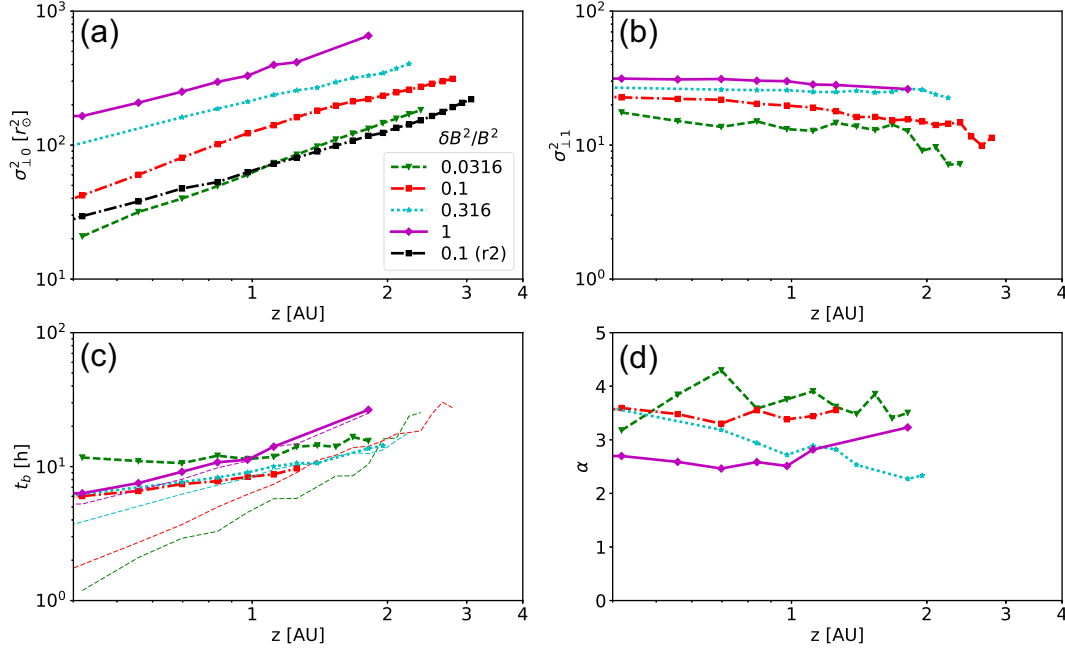


Figure 8. The fitting parameters of the equation (3) to the 10 MeV proton cross-field variances at different distances propagating in turbulence with different amplitudes $\delta B^2/B^2$ and $q_{\parallel} = 5/3$. (a) the early-time cross-field variance of the distribution, $\sigma_{\perp 0}^2$, with the black dash–dotted curve showing a different turbulence realization as compared to the red dash–dotted curve, for $\delta B^2/B^2 = 0.1$; (b) the asymptotic long-time behaviour $\sigma_{\perp 1}^2$; (c) the turnover time t_b (thick curves) and the asymptotic behaviour changing time t_a (thin dashed curves); and (d) the power-law index α .

dependence is now close to $\sigma_{\perp 1}^2 \propto p^{1.5}$. This dependence is again close to the NLGC prediction $\lambda_{\perp} \propto \lambda_{\parallel}^{1/3}$ which, together with the quasi-linear theory result $\lambda_{\parallel} \propto R^{2-q_{\parallel}}$ and $q_{\parallel} = 1$ gives $\kappa_{\perp} = v\lambda_{\perp}/3 \propto p^{4/3}$ at non-relativistic limit (Matthaeus et al. 2003; Shalchi et al. 2004).

In panel (c) of Fig. 7, we show the behaviour of the onset time t_b as a function of energy and distance. Compared to the $q_{\parallel} = 5/3$ case, the dependence of the onset time on energy is stronger, with $t_b \propto 1/v^{3/2}$. This is in contradiction with the suggestion that the time-scale would scale as the parallel scattering time (Laitinen & Dalla 2017), as this time-scale, λ_{\parallel}/v , would be constant for $q_{\parallel} = 1$. The discrepancy may be due to the strong parallel scattering of the particles for the $q_{\parallel} = 1$ case. In a strongly diffusive environment, the particles propagate in time-scales $t \propto z^2$, thus much slower for the scatter-dominated case of $q_{\parallel} = 1$, as compared to the almost scatter-free case with $q_{\parallel} = 5/3$. The slower parallel propagation implies that the finite propagation time effects, not accounted for in the simple diffusion model, are much more pronounced for the $q_{\parallel} = 1$ case.

In Fig. 8, we investigate the effect of varying turbulence amplitudes on the 10 MeV proton distribution extent across the mean field, with $q_{\parallel} = 5/3$, in the same format as in Figs 6 and 7. The turbulence at different amplitudes is obtained so that the random phases and polarizations of the Fourier modes were the same for each simulation, and only the amplitudes of the Fourier modes were changed.

Fig. 8(a) shows the dependence of the early-time constant cross-field extent $\sigma_{\perp 0}^2$ on the turbulence amplitude, from $\delta B^2/B^2 = 0.0316$ (dashed green curve) to $\delta B^2/B^2 = 1$ (solid magenta curve). The initial variance is proportional to the distance z along the mean field direction at all turbulence amplitudes, again consistent with particles propagating on diffusively meandering field lines. We found that $\sigma_{\perp 0}^2/z \propto \sqrt{\delta B^2/B^2}$, which is consistent with the dependence of the field line diffusion coefficient on the amplitude of the 2D-turbulence (Matthaeus et al. 1995).

In Fig. 8(a), we also show the early-time cross-field variance $\sigma_{\perp 0}^2$ for a simulation with $\delta B^2/B^2 = 0.1$ with random phases and polarizations different from the ones used in the other simulations presented in Fig. 8, with black dash–dotted curve. As can be seen, the two realizations with $\delta B^2/B^2 = 0.1$ (black and red dash–dotted curves) differ by factor 2. Thus, different realizations can locally produce significantly different turbulence conditions, which can affect parametric comparison of particle and field line dynamics in simulated turbulence. For this reason, it is important to keep consistency in the simulated fields when comparing, for example, the effect of turbulence amplitudes only on the particle transport, as in Fig. 8.

In Fig. 8(b), we see that the time-asymptotic diffusive spreading rate does not depend strongly on the turbulence amplitude. Upon closer inspection, we find that $\sigma_{\perp 1}^2$ from our fits is proportional to $(\delta B^2/B^2)^{0.25}$, which is slightly flatter than the dependence given by the NLGC value $\kappa_{\perp} \propto (\delta B^2/B^2)^{2/3} \kappa_{\parallel}^{1/3}$ (Shalchi et al. 2004), which for quasi-linear theory $\kappa_{\parallel} \propto (\delta B^2/B^2)^{-1}$ (Jokipii 1966) would give $\kappa_{\perp} \propto (\delta B^2/B^2)^{1/3}$. In our simulations, the dependence of κ_{\parallel} on turbulence amplitude, however, differed slightly from the quasi-linear theory value: using our κ_{\parallel} from the simulations in the NLGC expression we get $\kappa_{\perp} \propto (\delta B^2/B^2)^{0.2}$, close to the $\sigma_{\perp 1}^2 \propto (\delta B^2/B^2)^{0.25}$ obtained from our fits in Fig. 8(b). In addition, the recent work by Ruffolo et al. (2012) found a non-power law, flattening behaviour for κ_{\perp} at higher turbulence amplitudes, which may be visible also in our simulations.

In Fig. 8(c), we see that t_b decreases with increasing turbulence amplitude for the two lowest turbulence amplitudes (the green dashed curve and red dash–dotted curve), again consistent with the Laitinen & Dalla (2017) result. Subsequently, at higher amplitudes, the onset time begins to increase. The increase can in part be due to slow propagation times of the more diffusive particles in higher amplitude turbulence, as well as due to the asymptotic time t_a (the thin dashed curves) approaching t_b which, as discussed in

Appendix A, renders the fitting of the variance to equation (3) insensitive to the parameters t_b and α . The resulting spurious behaviour can also be seen in the fitted value of the power-law index, α , in Fig. 8(d).

4 DISCUSSION

Our analysis shows that the initial cross-field propagation of particles in turbulent magnetic fields is non-diffusive over a wide range of turbulence and particle parameters, reinforcing the conclusions made in the case study by Laitinen et al. (2013). Initially, particles remain on their field lines, as demonstrated by the energy-independent initial spreading of the particles in different turbulence environments (Figs 6a and 7a), which is followed by a time-asymptotic, energy-dependent diffusive spreading of the particles across the mean field direction. The early-time constant cross-field variance phase is seen as a very fast access of particles to wide cross-field ranges, and it lasts for hours to tens of hours depending on particle and turbulence parameters.

We found that the early-time cross-field extent of the particle population, as given by the cross-field variance $\sigma_{\perp 0}^2$ in equation (3), is proportional to the distance z from the particle source along the mean field direction, and $\sqrt{\delta B^2/B^2}$. Thus, the initial propagation phase is consistent with particles propagating along diffusively meandering field lines in turbulence dominated by 2D wave modes (Matthaeus et al. 1995). At the time-asymptotic limit, the rate of cross-field spreading obtained in our simulations can be described as diffusion with cross-field diffusion coefficient κ_{\perp} proportional to velocity (for the $q_{\parallel} = 5/3$ case) and $(\delta B^2/B^2)^{0.25}$, consistent with the our current theoretical understanding of asymptotic particle cross-field diffusion (e.g. Matthaeus et al. 2003; Shalchi et al. 2004; Ruffolo et al. 2012). Thus, the early-time and the time-asymptotic phases of the particle cross-field propagation in our simulations are consistent with our theoretical understanding of the field line and particle behaviour at the corresponding limits.

Our study shows that the transition between the early spreading along the meandering field lines, and the time asymptotic diffusion phase does not follow the simple diffusion picture presented in equation (A5) in most cases studied in this work, but suggests a delayed onset of the diffusion phase after fast expansion, as indicated by the recent results by Laitinen & Dalla (2017). As discussed in Appendix A, assuming particles to diffuse from the meandering field lines at a constant rate (magenta curve in Fig. A1) can result in overestimation of the cross-field variance of the particle population by up to a factor of 2 during the transition phase between the initial and time-asymptotic propagation phases. We find that for low-scattering conditions, the onset of the time-asymptotic phase, t_b , follows approximately the dependence on the parallel scattering rate obtained by Laitinen & Dalla (2017). For stronger turbulence, however, the scaling does not hold any more, possibly due to finite propagation time effects, which are not contained in our simple model behind the formulation of equation (3). The particles may have also been already decoupled from their fieldlines before reaching distance z , which would result in inaccuracy in the determination of t_b , as discussed in Appendix A.

5 CONCLUSIONS

In this work, we have studied how the turbulence and particle properties affect the particle spreading across the mean field direction early after the particle release. Our results show that

(i) Initially, the particles spread systematically and rapidly to a wide cross-field range along meandering field lines. They remain on the fieldlines from hours up to tens of hours for protons of 1–100 MeV, in turbulence consistent with those measured during SEP events (e.g. Palmer 1982; Torsti et al. 2004) and interplanetary turbulence conditions (e.g. Pei et al. 2010; Laitinen et al. 2016; Strauss et al. 2017).

(ii) The late-time behaviour of the particles is consistent with energy-dependent cross-field diffusion, and is consistent with the current theoretical understanding of the time-asymptotic cross-field diffusion of particles in turbulent magnetic fields (e.g. Matthaeus et al. 2003; Shalchi et al. 2004; Ruffolo et al. 2012).

(iii) The transition between the initial and time-asymptotic behaviour can be roughly modelled as a simple spatial diffusion of particles from their meandering field lines. More precise modelling reveals a delayed decoupling of particles from the meandering field lines, as demonstrated in Laitinen & Dalla (2017).

Thus, our study shows that over a wide range of turbulence and particle parameters SEP cross-field propagation cannot be modelled by cross-field diffusion alone early in the SEP event, but the systematic propagation along meandering field lines must be taken into account. Simple models, such as the one applied in Laitinen et al. (2016), that model the particle distribution evolution as cross-field diffusion of particles from meandering field lines provide a significant improvement as compared to the earlier models diffusing particles with respect to the mean magnetic field. Future fully consistent cross-field propagation models should also include the time-scales related to the decoupling of the particles from the meandering field lines (Laitinen & Dalla 2017). For early-time evolution of the particle populations, a time-dependent diffusion coefficient, such as used in equation (A6), may prove useful. We will investigate advanced modelling of cross-field particle propagation in a future work.

ACKNOWLEDGEMENTS

TL and SD acknowledge support from the UK Science and Technology Facilities Council (STFC) (grants ST/J001341/1 and ST/M00760X/1) and the International Space Science Institute as part of international team 297. D. Marriot was funded by the Royal Astronomical Society. This work used the DiRAC Complexity system, operated by the University of Leicester IT Services, which forms part of the STFC DiRAC HPC Facility (www.dirac.ac.uk). This equipment is funded by BIS National E-Infrastructure capital grant ST/K000373/1 and STFC DiRAC Operations grant ST/K0003259/1. DiRAC is part of the National E-Infrastructure. Access to the University of Central Lancashire's High Performance Computing Facility is gratefully acknowledged.

REFERENCES

- Cohen C. M. S., Mason G. M., Mewaldt R. A., Wiedenbeck M. E., 2014, *ApJ*, 793, 35
 Dresing N., Gómez-Herrero R., Klassen A., Heber B., Kartavykh Y., Dröge W., 2012, *Sol. Phys.*, 281, 281
 Dresing N., Gómez-Herrero R., Heber B., Klassen A., Malandraki O., Dröge W., Kartavykh Y., 2014, *A&A*, 567, A27
 Dröge W., Kartavykh Y. Y., Klecker B., Kovaltsov G. A., 2010, *ApJ*, 709, 912
 Fraschetti F., Jokipii J. R., 2011, *ApJ*, 734, 83
 Giacalone J., Jokipii J. R., 1999, *ApJ*, 520, 204

- Giacalone J., Jokipii J. R., 2012, ApJ, 751, L33
 He H.-Q., Qin G., Zhang M., 2011, ApJ, 734, 74
 Jokipii J. R., 1966, ApJ, 146, 480
 Laitinen T., Dalla S., 2017, ApJ, 834, 127
 Laitinen T., Dalla S., Kelly J., 2012, ApJ, 749, 103
 Laitinen T., Dalla S., Marsh M. S., 2013, ApJ, 773, L29
 Laitinen T., Kopp A., Effenberger F., Dalla S., Marsh M. S., 2016, A&A, 591
 Lario D., Aran A., Gómez-Herrero R., Dresing N., Heber B., Ho G. C., Decker R. B., Roelof E. C., 2013, ApJ, 767, 41
 Marsh M. S., Dalla S., Kelly J., Laitinen T., 2013, ApJ, 774, 4
 Matthaeus W. H., Gray P. C., Pontius D. H., Jr, Bieber J. W., 1995, Phys. Rev. Lett., 75, 2136
 Matthaeus W. H., Qin G., Bieber J. W., Zank G. P., 2003, ApJ, 590, L53
 Palmer I. D., 1982, Rev. Geophys. Space Phys., 20, 335
 Parker E. N., 1965, Planet. Space Sci., 13, 9
 Pei C., Bieber J. W., Breech B., Burger R. A., Clem J., Matthaeus W. H., 2010, J. Geophys. Res. (Space Physics), 115, A03103
 Qin G., Wang Y., Zhang M., Dalla S., 2013, ApJ, 766, 74
 Richardson I. G. et al., 2014, Sol. Phys., 289, 3059
 Ruffolo D., Pianpanit T., Matthaeus W. H., Chuychai P., 2012, ApJ, 747, L34
 Shalchi A., 2010, ApJ, 720, L127
 Shalchi A., Bieber J. W., Matthaeus W. H., 2004, ApJ, 604, 675
 Strauss R. D. T., Dresing N., Engelbrecht N. E., 2017, ApJ, 837, 43
 Tautz R. C., 2012, J. Comput. Phys., 231, 4537
 Tautz R. C., Shalchi A., Dosch A., 2011, J. Geophys. Res. (Space Physics), 116, A02102
 Tooprakai P., Seripienlert A., Ruffolo D., Chuychai P., Matthaeus W. H., 2016, ApJ, 831, 195
 Torsti J., Riihonen E., Kocharov L., 2004, ApJ, 600, L83
 Wiedenbeck M. E., Mason G. M., Cohen C. M. S., Nitta N. V., Gómez-Herrero R., Haggerty D. K., 2013, ApJ, 762, 54
 Zhang M., Qin G., Rassoul H., 2009, ApJ, 692, 109

APPENDIX A: THE WIDTH OF A DISTRIBUTION IN A SIMPLE DIFFUSION PICTURE

If we exclude the finite propagation time effects on particle propagation, the diffusive spreading of a particle population along and across the mean field can be described as spatial diffusion as

$$\frac{\partial n_{3D}}{\partial t} = \nabla \cdot \hat{\kappa} \nabla n_{3D}, \quad (\text{A1})$$

where n_{3D} is the density of the particles and the non-zero elements of the diffusion tensor $\hat{\kappa}$ are $\kappa_{xx} = \kappa_{yy} \equiv \kappa_{\perp}$ and $\kappa_{zz} \equiv \kappa_{\parallel}$. For impulsive point-source injection, the solution to the diffusion equation is

$$n_{3D}(r, t) = \frac{I_0}{(4\kappa_{\perp}^2 \kappa_{\parallel} t)^{3/2}} \exp \left\{ -\frac{x^2 + y^2}{4\kappa_{\perp} t} - \frac{z^2}{4\kappa_{\parallel} t} \right\}. \quad (\text{A2})$$

Taking the second moment of this with respect to x , we find for the variance in the x -direction

$$\sigma_x^2(t, y, z) = 2\kappa_{\perp} t \quad (\text{A3})$$

Thus, for an impulsive injection and pure diffusion, the variance of the particle population at all z grows linearly with time.

Laitinen et al. (2013) showed that cross-field diffusion does not describe the particle cross-field distribution early in the event and concluded that the particles follow the meandering field lines systematically, and diffuse from them slowly. To describe such behaviour, we consider as the first approach a simple model where the particles are initially distributed in the cross-field x -direction on a

Gaussian distribution with $\sigma^2 = 2zD_{FL}$, where D_{FL} is the diffusion coefficient for the field lines, mimicking the cross-field distribution of particles that propagate along turbulently meandering field lines. Subsequently, the particles spread diffusively in the x -direction from their field lines. As we ignore the propagation along the field lines in this simple model, we can describe the evolution of the particle density as

$$\frac{\partial n_{1D}(x, z, t)}{\partial t} = \frac{\partial}{\partial x} \kappa_{\perp} \frac{\partial n_{1D}(x, z, t)}{\partial x}, \quad (\text{A4})$$

which, for the Gaussian initial condition, yields for the cross-field variance

$$\sigma_{\perp}^2(t, z) = 2zD_{FL} + 2\kappa_{\perp} t. \quad (\text{A5})$$

We show the behaviour of the cross-field variance given by equation (A5) in Fig. A1 with the solid magenta curve, comparing it with a simulation case with 100 MeV protons at 0.56 au along the mean field direction, with turbulence variance $\delta B^2/B^2 = 0.1$ and $q_{\parallel} = 5/3$. The first and second term in equation (A5) are shown with the black and magenta dashed curves, respectively, and the intercept time of the terms, t_a , shown with the magenta diamond. As can be seen, the magenta curve does not trace the simulation result, solid black curve, well during the transition phase.

Recently, Laitinen & Dalla (2017) noted that the decoupling of particles from their initial field lines is initially slow, and only at later times rapidly converges to the time-asymptotic diffusion trend. Such a behaviour can be mimicked by allowing time-dependence for the particle diffusion coefficient, with $\kappa_{\perp}(t) = \kappa_{\perp 0} T(t)$. Substituting $d\tau = T(t) dt$, we can solve the equation (A4) for $\kappa_{\perp}(t)$, which results, for impulsive point source, in variance $\sigma_x^2(t) = 2\kappa_{\perp 0} \tau(t)$, and for a Gaussian initial condition in

$$\sigma_{\perp}^2(t, z) = 2zD_{FL} + 2\kappa_{\perp 0} \tau(t). \quad (\text{A6})$$

We demonstrate the use of the solution given by equation (A6), parametrized as in equation (3), in Fig. A1, for the simulated case of 100 MeV protons at 0.56 au along the mean field direction.

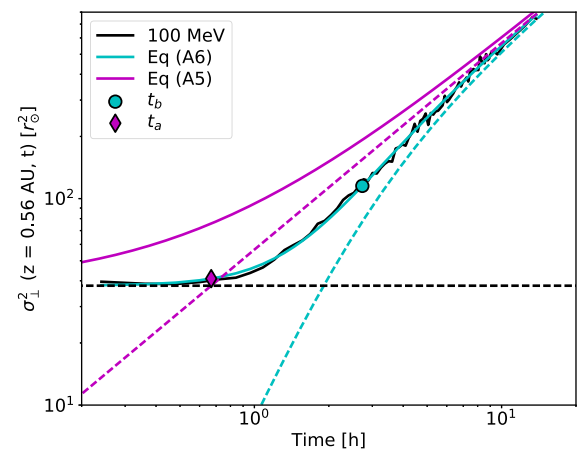


Figure A1. The cross-field variance of 100 MeV protons at 0.56 au, with turbulence parameters $\delta B^2/B^2 = 0.1$ and $q_{\parallel} = 5/3$. The solid magenta curve shows the fit to equation (A5) and the solid cyan curve to equation (A6), using the functional shape given in equation (3). The black dashed line shows the asymptotic $\sigma_{\perp}^2(t, z) = \sigma_{\perp 0}$, the dashed cyan curve shows the second term in equation (3) and the dashed magenta curve shows the asymptotic $\sigma_{\perp}^2(t, z) = \sigma_{\perp 1} t / t_0$. The magenta diamond shows the intercept of the asymptotes, $t_a = \sigma_{\perp 0} / \sigma_{\perp 1} t_0$ and the cyan circle shows the t_b .

turbulence variance $\delta B^2/B^2 = 0.1$ and $q_{\parallel} = 5/3$. As can be seen, the equation (A6) describes the time evolution of the simulation results well.

When fitting the $\sigma_{\perp}^2(z, t)$ from the simulations to equation (3), the difference between the simple approach, equation (A3), and equation (3), is not always as clear as in Fig. A1. If the $t_b \ll t_a$, the second term in equation (3) approaches $\sigma_{\perp 1}^2(z)t/t_0$, and is longer

sensitive to parameters t_b and α . The $t_b \ll t_a$ implies that the onset of the diffusive phase has taken place before the particles have reached the distance z .

To avoid showing the spurious fit parameters, we show the fit parameters t_b and α only when $t_b \geq t_a$ in Figs (6)–(8).

This paper has been typeset from a \TeX/L\AA\TeX file prepared by the author.